

A python package for ultrashort optical pulse propagation in terms of forward models for the analytic signal

O. Melchert^{a,b,*}, A. Demircan^{a,b}

^a*Institute of Quantum Optics, Leibniz Universität Hannover, Welfengarten 1, 30167 Hannover, Germany*

^b*Cluster of Excellence PhoenixD (Photonics, Optics, and Engineering - Innovation Across Disciplines), Welfengarten 1, Hannover, Germany*

Abstract

We present a flexible, open-source Python package for the accurate simulation of the z -propagation dynamics of ultrashort optical pulses in nonlinear waveguides, especially valid for few-cycle pulses and their interaction. The simulation approach is based on unidirectional propagation equations for the analytic signal. The provided software allows to account for dispersion, attenuation, four-wave mixing processes including, e.g., third-harmonic generation, and features various models for the Raman response. The propagation equations are solved on a periodic temporal domain. For z -propagation, a selection of pseudospectral methods is available. Propagation scenarios for a custom propagation constant and initial field pulses can either be specified in terms of a HDF5 based input file format or by direct implementation using a python script. We demonstrate the functionality for a test-case for which an exact solution is available, by reproducing exemplary results documented in the scientific literature, and a complex propagation scenario involving multiple pulses. The `py-fmas` code, its reference manual, an extended user guide, and further usage examples are available online at <https://github.com/omelchert/py-fmas>.

Contents

1	Introduction	1	7	Software documentation	8
2	Propagation models for the analytic signal	2	8	Software extendibility	8
3	Computational problem solved by the software	3	9	Usage examples	8
4	Implemented algorithms	3	9.1	Exact single-soliton solution of the NSE	8
4.1	Available z -stepping formulas	4	9.2	Supercontinuum generation in a PCF	9
4.2	Simple split-step Fourier method (SiSSM)	4	9.3	Interaction of four pulses in a ESM fiber	10
4.3	Symmetric split-step Fourier method (SySSM)	4	Appendix A	Recognized input-file parameters	11
4.4	Integrating factor method (IFM)	4	Appendix B	Computing spectrograms	11
4.5	Local-error method (LEM)	4	Appendix C	Raman response functions	11
4.6	Conservation quantity error method (CQE)	5	Appendix D	Analyzing propagation constants	12
5	User manual	5	Acknowledgements		13
5.1	Structure of the <code>py-fmas</code> package	5	References		13
5.2	Availability of the software	6	1. Introduction		
5.3	Specifying a propagation scenario	6	The accurate theoretical description of the propagation dynamics of ultrashort optical pulses in nonlinear media requires flexible models, adaptable to a wide variety of experimental conditions, and accurate approximation methods, facilitating the dynamical evolution of the optical field. Typically considered models are, e.g., the forward Maxwell equation [1], or nonlinear envelope equations [2], such as the generalized nonlinear Schrödinger equation [3, 4, 5].		
5.4	Initializing a model	6			
5.5	Initializing a solver and running a simulation	6			
5.6	Data storage	7			
5.7	Using <code>fmas</code> as application	7			
5.8	Data postprocessing	7			
6	Software dependencies	7			

*Corresponding author

Email addresses: melchert@iqo.uni-hannover.de (O. Melchert), demircan@iqo.uni-hannover.de (A. Demircan)

Here, we introduce `py-fmas`, a Python package for the accurate numerical simulation of the complex propagation dynamics of ultrashort optical pulses in nonlinear waveguides, especially valid for few-cycle pulses and propagation scenarios involving multiple pulses with distinct frequencies. The considered z -propagation models are formulated in terms of the complex-valued analytic signal related to the real-valued optical field [6, 7, 8, 9, 10]. Description of the field dynamics in terms of the analytic signal has several advantages. For example, it allows to directly neglect non-resonant contributions of four-wave mixing [7], and to derive models that are formally simpler than the forward Maxwell equation [1]. Still, additional nonlinear effects such as the Raman effect can be included in a standard way [10, 9]. A further advantage of these models is that they are exempt from the slowly varying envelope approximation (SVEA) commonly adopted for the derivation of nonlinear Schrödinger type equations. This limits the applicability of the latter models for the accurate simulation of few-cycle pulses which do not satisfy the SVEA [11, 12]. Nevertheless, as prominent limiting case, the envelope-based generalized nonlinear Schrödinger equation [3, 4, 5], including all its usual effects, can be obtained from analytic signal based models [6]. For the dynamical evolution of the analytic signal, `py-fmas` provides a selection of propagation algorithms commonly used in nonlinear optics for the solution of nonlinear Schrödinger type equations.

The remainder of the article is organized as follows. In sect. 2 we introduce the considered propagation models, and in sect. 3 we state the computational problem solved by the provided software. In sect. 4 we detail the implemented numerical methods. In sect. 5 we provide a brief user manual that guides the reader through a workflow using the `py-fmas` library code. In sects. 6–8 we discuss the dependencies of the software and software extensibility, and in sect. 9 we illustrate three usage examples. Additional features of the provided software are discussed in the appendix. In particular, Appendix B discusses the capability to compute spectrograms, Appendix C details the various implemented Raman response models, and Appendix D illustrates a convenience class for handling and analyzing propagation constants. The `py-fmas` code, a reference manual, an extended user guide and several usage examples are available online at <https://github.com/omelchert/py-fmas> [13].

2. Propagation models for the analytic signal

We here consider a periodic sequence of linearly polarized electromagnetic pulses propagation along the z -direction of a one-dimensional dispersive and nonlinear medium, supporting single-mode propagation [6, 7]. Let

$$E(z, t) = \mathcal{F}^{-1} [E_\omega(z)] = \sum_{\omega} E_\omega(z) e^{-i\omega t}, \quad \omega \in \frac{2\pi}{T} \mathbb{Z}, \quad (1)$$

denote the corresponding real-valued field in a temporal domain of period $T = 2t_{\max}$, with

$$E_\omega(z) = \mathcal{F} [E(z, t)] = \frac{1}{T} \int_{-t_{\max}}^{t_{\max}} E(z, t) e^{i\omega t} dt, \quad (2)$$

where $E_\omega = E_{-\omega}^*$. The average field is considered to be constant along the z -direction, assuming $E_{\omega=0}(z) = 0$. Above, \mathcal{F} and \mathcal{F}^{-1} denote the forward and inverse Fourier transform. Then, under conditions that are common in optical fibers the field of the pulse sequence can be described in terms of the nonlinear first-order z -propagation equation [6, 7]

$$i\partial_z E_\omega + [\beta(\omega) + i\alpha(\omega)] E_\omega + \frac{\omega^2 \chi}{2c^2 \beta(\omega)} \sum_{123|\omega} E_{\omega_1} E_{\omega_2} E_{\omega_3} = 0, \quad (3)$$

where c is the speed of light, χ is a constant nonlinear susceptibility specifying a cubic Kerr model, and the sum-index token $123|\omega$ abbreviates the condition $\omega_1 + \omega_2 + \omega_3 = \omega$. In Eq. (3), the frequency dependent propagation constant β and attenuation factor α specify the real-valued odd and even parts of the complex valued wave number $k(\omega) = \beta(\omega) + i\alpha(\omega) = \omega \sqrt{\epsilon(\omega)}/c$, related to the dielectric constant ϵ . The propagation constant relates to the refractive index $n(\omega) = \text{Re}[\sqrt{\epsilon(\omega)}]$ in the form $\beta(\omega) = \omega n(\omega)/c$.

Based on the above unidirectional propagation model for the field, a sequence of simplified models can be derived that have the advantage of directly neglecting non-resonant contributions of four-wave mixing in the nonlinear part of Eq. (3). This is achieved by considering, instead of the real optical field $E(z, t)$, the complex-valued analytic signal

$$\mathcal{E}(z, t) = \sum_{\omega>0} \mathcal{E}_\omega(z) e^{i\omega t}, \quad \mathcal{E}_\omega(z) = [1 + \text{sign}(\omega)] E_\omega(z), \quad (4)$$

with $\mathcal{E}_{\omega<0} = 0$. The optical field is related to the analytic signal by $E = (\mathcal{E} + \mathcal{E}^*)/2 = \text{Re}[\mathcal{E}]$. Using Eq. (4), the propagation equation for the analytic signal, derived from Eq. (3), reads [10]

$$i\partial_z \mathcal{E}_\omega + k(\omega) \mathcal{E}_\omega + \frac{\omega^2 \chi}{8c^2 \beta(\omega)} ((\mathcal{E} + \mathcal{E}^*)^3)_{\omega>0} = 0, \quad (5)$$

wherein $[\cdot]_{\omega>0}$ denotes spectral components restricted to the positive frequency part of the nonlinearity. In terms of this analytic signal, all four-wave-mixing (FWM) processes that enter Eq. (3) can be separated. Specifically we can separate the field product in the nonlinear part according to

$$(\mathcal{E} + \mathcal{E}^*)^3 = \mathcal{E}^3 \quad (6a)$$

$$+ 3|\mathcal{E}|^2 \mathcal{E} \quad (6b)$$

$$+ 3|\mathcal{E}|^2 \mathcal{E}^* \quad (6c)$$

$$+ \mathcal{E}^{*3}, \quad (6d)$$

where Eq. (6a) facilitates third-harmonic generation (THG), Eq. (6b) is a Kerr-type nonlinear term, Eq. (6c) is a conjugate Kerr-type term, and Eq. (6d) can be neglected when restricting to $\omega > 0$ in Eq. (5). Considering only FWM processes defined by Eq. (6b), Eq. (5) simplifies to [7, 6]

$$i\partial_z \mathcal{E}_\omega + k(\omega) \mathcal{E}_\omega + \frac{3\omega^2 \chi}{8c^2 \beta(\omega)} (|\mathcal{E}|^2 \mathcal{E})_{\omega>0} = 0, \quad (7)$$

which we here refer to as the forward model for the analytic signal (implemented as model FMAS). Further, we here refer

to Eq. (5) as the forward model for the analytic signal including terms such as third-harmonic generation (implemented as model FMAS_THG).

Additional simplification of the nonlinear term is possible by approximating $\beta(\omega) \approx \omega n(\omega_0)/c$ for a reference frequency ω_0 , and by expressing the nonlinear susceptibility χ through the nonlinear refractive index n_2 as $\chi = \frac{8}{3}n(\omega_0)n_2$. Then, Eq. (7) can be written in the form [10, 9]

$$i\partial_z \mathcal{E}_\omega + k(\omega)\mathcal{E}_\omega + n_2 \frac{\omega}{c} (|\mathcal{E}|^2 \mathcal{E})_{\omega>0} = 0, \quad (8)$$

yielding a simplified forward model for the analytic signal (implemented as model FMAS_S).

The Raman effect is incorporated by augmenting the nonlinear part in the form [10, 9]

$$i\partial_z \mathcal{E}_\omega + k(\omega)\mathcal{E}_\omega + n_2 \frac{\omega}{c} \left((1-f_R)|\mathcal{E}|^2 \mathcal{E} + f_R \mathcal{E} \mathcal{I}_R \right)_{\omega>0} = 0, \quad (9)$$

where f_R specifies the fractional Raman contribution, and

$$\mathcal{I}_R = \sum_{\omega} h(\omega) (|\mathcal{E}|^2)_{\omega} e^{-i\omega t}, \quad h(\omega) = \frac{\tau_1^{-2} + \tau_2^{-2}}{\tau_1^{-2} - (\omega + i\tau_2^{-1})^2}, \quad (10)$$

represents convolution with a generic two parameter Raman response function $h(\omega)$. The latter implements an approximation by a single-damped-harmonic oscillator with parameters $\tau_{1,2}$. For example, for silica fibers adequate values are $f_R = 0.18$, $\tau_1 = 12.2$ fs, and $\tau_2 = 32$ fs. More specific expressions for the response function $h(\omega)$ might of course be used, see Appendix C. Equation (9) comprises the simplified forward model for the analytic signal including the Raman effect (implemented as model FMAS_S_R).

Subsequently, so as to assess the accuracy of our numerical simulations in the no-loss limit ($\alpha = 0$), we consider the conserved quantities

$$C_p(z) = \begin{cases} \sum_{\omega>0} \omega^{-2} \beta(\omega) |\mathcal{E}_\omega(z)|^2, & \text{for Eqs. (5,7),} \\ \sum_{\omega>0} \omega^{-1} |\mathcal{E}_\omega(z)|^2, & \text{for Eqs. (8,9),} \end{cases} \quad (11)$$

which are related to the classical analog of the photon number, see Refs. [6, 8] for Eqs. (5,7), and Refs. [14, 15, 16] for models with nonlinearity of the form of Eqs. (8,9).

3. Computational problem solved by the software

The computational problem solved by the provided software is an initial value problem, consisting of the propagation of a complex-valued field $\mathcal{E}(z, t)$ along the propagation coordinate z on a periodic t -domain of extend $T = 2t_{\max}$, governed by a nonlinear partial differential equation (PDE) of first order, i.e.

$$\partial_z \mathcal{E}(z, t) = L\mathcal{E}(z, t) + N(\mathcal{E}(z, t)), \quad z \geq 0, |t| \leq t_{\max}, \quad (12a)$$

$$\mathcal{E}(z, -t_{\max}) = \mathcal{E}(z, t_{\max}) \quad z \geq 0, \quad (12b)$$

$$\mathcal{E}(z, t)|_{z=0} = \mathcal{E}_0(t) \quad |t| \leq t_{\max}. \quad (12c)$$

In Eq. (12a), L and N are linear and nonlinear operators, respectively. Equation (12b) specifies the boundary conditions,

and Eq. (12c) specifies the initial condition. Taking the Fourier transform of Eq. (12a) we obtain the equation

$$\partial_z \mathcal{E}_\omega(z) = \hat{L}(\omega)\mathcal{E}_\omega(z) + \hat{N}(z), \quad (13)$$

where $\mathcal{E}_\omega(z) = \mathcal{F}[\mathcal{E}(z, t)]$, $\hat{L}(\omega) = ik(\omega)$, and $\hat{N}(z) = \mathcal{F}[N(\mathcal{E}(z, t))]$. The models defined by Eqs. (5, 7, 8, 9), are conveniently expressed in the generic form of Eq. (13), see Tab. 1, which allows for effective pseudospectral implementations. The z -propagation algorithms implemented in `py-fmas` are discussion in sect. 4 below.

Table 1

List of implemented models. Propagation equations are specified using the frequency domain representation of their linear ($\hat{L}(\omega)$) and nonlinear (\hat{N}) operators in the form of Eq. (13). A conserved quantity, related to the classical expression for the photon number, valid in the no-loss limit ($\alpha = 0$), is implemented by default (C_p).

Model	$\hat{L}(\omega)$	$\hat{N}(z)$	$C_p(z)$
FMAS_THG	$ik(\omega)$	$i \frac{3\omega^2 \chi}{8c^2 \beta(\omega)} (\mathcal{E} + \mathcal{E}^*)^3_{\omega>0}$	$\sum_{\omega>0} \frac{\beta(\omega)}{\omega^2} \mathcal{E}_\omega ^2$
FMAS	$ik(\omega)$	$i \frac{3\omega^2 \chi}{8c^2 \beta(\omega)} (\mathcal{E} ^2 \mathcal{E})_{\omega>0}$	$\sum_{\omega>0} \frac{\beta(\omega)}{\omega^2} \mathcal{E}_\omega ^2$
FMAS_S	$ik(\omega)$	$i \frac{n_2 \omega}{c} (\mathcal{E} ^2 \mathcal{E})_{\omega>0}$	$\sum_{\omega>0} \omega^{-1} \mathcal{E}_\omega ^2$
FMAS_S_R	$ik(\omega)$	$i \frac{n_2 \omega}{c} ((1-f_R) \mathcal{E} ^2 \mathcal{E} + f_R \mathcal{E} \mathcal{I}_R)_{\omega>0}$	$\sum_{\omega>0} \omega^{-1} \mathcal{E}_\omega ^2$
		$\mathcal{I}_R = \sum_{\omega} h(\omega) (\mathcal{E} ^2)_{\omega} e^{-i\omega t}$	

4. Implemented algorithms

A commonality of the above models is that their linear subproblem can be solved by direct integration. That is, if only the linear part of Eq. (13) is nonzero, an exact solution is given by $\mathcal{E}_\omega(z) = \mathbf{P}_{\text{lin}}(z) \mathcal{E}_\omega(0)$. In the latter,

$$\mathbf{P}_{\text{lin}}(z) = e^{\hat{L}(\omega)z} \quad (14)$$

is the exact linear propagator for advancing \mathcal{E}_ω under the action of the linear operator. In this case, a solution to Eq. (12a) can be computed as $\mathcal{E}(z, t) = \mathbf{F}^{-1}[\mathbf{P}_{\text{lin}}(z) \mathcal{F}[\mathcal{E}(0, t)]]$. All propagation schemes implemented in `py-fmas` module `solver` exploit the above property.

To advance a field for a single step along a discrete z -grid, three fixed-stepsize algorithms are implemented. These are the simple split-step Fourier method (SiSSM; sect. 4.2), symmetric split-step Fourier method (SySSM; sect. 4.3), and integrating factor method (IFM; sect. 4.4). `py-fmas` also implements two adaptive stepsize algorithms, referred to as the local error method (LEM; sect. 4.5) and the conservation quantity error (CQE; sect. 4.6) method, where a single step of extend Δz possibly requires several substeps of the solver. Both methods aim at keeping the local error smaller than a prescribed error bound by decreasing the stepsize when necessary while increasing the stepsize when possible.

4.1. Available z -stepping formulas

A z -stepping formula implements the algorithmic procedure to advance a field for a single step from position z to $z + \Delta z$. This is important for solving the nonlinear subproblem of the considered models. Let z_n and y_n be the z -position and field after step n , then taking a single step can be abbreviated as

$$y_{n+1} = \mathbf{S}(f, z_n, y_n, \Delta z), \quad (15)$$

where $f = dy/dz$ is the evolution rate of the system to be solved and Δz is the step-size to be used. `py-fmas` provides functions implementing a second-order Runge-Kutta formula (RK2; local error $O(\Delta z^3)$) and fourth-order Runge-Kutta formula (RK4; local error $O(\Delta z^5)$) [17]. In Eq. (15), y not necessarily refers to the analytic signal. For example, the integrating factor method (sect. 4.4) advances an auxiliary field that is different from the analytic signal.

4.2. Simple split-step Fourier method (SiSSM)

In terms of the simple split-step Fourier method [18, 19], we advance a solution from z to $z + \Delta z$ by a subsequent composition of a nonlinear and a linear substep in the form

$$\xi = \mathbf{S}(\hat{N}, z, \mathcal{E}_\omega(z), \Delta z), \quad (16a)$$

$$\mathcal{E}_\omega(z + \Delta z) = \mathbf{P}_{\text{lin}}(\Delta z) \xi. \quad (16b)$$

The maximally achievable local error of this integration scheme is $O(\Delta z^2)$. The maximally achievable global error, accumulated over the full propagation range, is thus $O(\Delta z)$. A solver based on the above method is implemented as SiSSM (in the text referred to as SiSSM). By default it employs the RK2 z -stepping formula.

4.3. Symmetric split-step Fourier method (SySSM)

For the symmetric split-step Fourier method [20], we advance the solution from position z to $z + \Delta z$ by a subsequent composition of a linear half-step, a full nonlinear step, and a final linear half step in the form

$$\xi = \mathbf{P}_{\text{lin}}(\Delta z/2) \mathcal{E}_\omega(z), \quad (17a)$$

$$\xi' = \mathbf{S}(\hat{N}, z, \xi, \Delta z), \quad (17b)$$

$$\mathcal{E}_\omega(z + \Delta z) = \mathbf{P}_{\text{lin}}(\Delta z/2) \xi'. \quad (17c)$$

This integration scheme yields a maximal achievable global error $O(\Delta z^2)$. A solver based on the above method is implemented as SySSM (in the text referred to as SySSM). By default it employs the RK2 z -stepping formula.

4.4. Integrating factor method (IFM)

Starting with the generic partial differential equation in the frequency domain, Eq. (13), we define the auxiliary fields

$$\phi_\omega(z) = \mathbf{P}_{\text{lin}}(z_0 - z) \mathcal{E}_\omega(z), \quad (18)$$

where $\mathbf{P}_{\text{lin}}(z_0 - z) = \exp\{\hat{L}(\omega)(z_0 - z)\}$ specifies the integrating factor and z_0 is a reference position [22, 24]. Replacing \mathcal{E}_ω in

Eq. (13) by these auxiliary fields eliminates the linear part and yields a system of ordinary differential equations [22, 23, 24]

$$\partial_z \phi_\omega(z) = \mathbf{P}_{\text{lin}}(z_0 - z) \hat{N}(\mathbf{P}_{\text{lin}}(z - z_0) \phi_\omega(z)) \quad (19a)$$

$$= \hat{G}_{z_0}(z, \phi_\omega(z)), \quad (19b)$$

coupled through the nonlinear function \hat{G}_{z_0} . Equation (19b) defines an ‘‘interaction picture’’ representation of Eq. (13): in absence of an ‘‘interaction’’, i.e. if only the linear part of Eq. (13) is nonzero, the auxiliary fields satisfy $\partial_z \phi_\omega = 0$. In order to advance the original field from z to $z + \Delta z$, we here choose the reference position $z_0 = z + \Delta z/2$ in Eqs. (18, 19b). For this choice, the midpoint derivative for the auxiliary field matches that of the original field. A full step of the integrating factor method is then given by the composition

$$\phi_\omega(z) = \mathbf{P}_{\text{lin}}(\Delta z/2) \mathcal{E}_\omega(z), \quad (20a)$$

$$\xi = \mathbf{S}(\hat{G}_{z_0=z+\Delta z/2}, z, \phi_\omega(z), \Delta z), \quad (20b)$$

$$\mathcal{E}_\omega(z + \Delta z) = \mathbf{P}_{\text{lin}}(\Delta z/2) \xi. \quad (20c)$$

Equation (20a) performs the change to the auxiliary field at position z using Eq. (18), Eq. (20b) advances the auxiliary field using Eq. (19b), and Eq. (20c) recovers the original field at $z + \Delta z$, again using Eq. (18). For the above choice of the reference position z_0 , the sequence of substeps Eqs. (20a-20c) has a structure similar to the SySSM scheme [Eqs. (17a-17c)]. However, using the RK4 algorithm for z -stepping in Eq. (20b) results in a global error $O(\Delta z^4)$. The above variant of the integrating factor method is referred to as the ‘‘Runge-Kutta in the interaction picture’’ (RK4IP) method [25]. Such schemes are also referred to as linearly exact Runge-Kutta methods [21]. A solver based on the above procedure is implemented as IFM-RK4IP (in the text referred to as IFM-RK4IP).

4.5. Local-error method (LEM)

The second-order accurate symmetric split-step method (SySSM; sect. 4.3) can be used to devise a refined algorithm with local error $O(\Delta z^4)$ [26]. This can be achieved by step-doubling and local extrapolation [17]. To advance a solution from position z to $z + h$, step-doubling proceeds by computing a coarse solution $\mathcal{E}_\omega^{(c)}(z + h)$ using a full step of extend h , and a fine solution $\mathcal{E}_\omega^{(f)}(z + h)$ using a subsequent composition of two half-steps of extend $h/2$. Local extrapolation consists of combining the results in the form [26]

$$\mathcal{E}_\omega(z + h) = \frac{4}{3} \mathcal{E}_\omega^{(f)}(z + h) - \frac{1}{3} \mathcal{E}_\omega^{(c)}(z + h). \quad (21)$$

In comparison to the number of evaluations of Eq. (17b) needed to compute the fine solution, the overhead cost for evaluating Eq. (21) is a factor 1.5.

In the local-error method [26], the relative local error

$$\delta_{\text{RLE}} = \frac{\|\mathcal{E}_\omega^{(f)} - \mathcal{E}_\omega^{(c)}\|}{\|\mathcal{E}_\omega^{(f)}\|}, \quad (22)$$

with norm $\|x\| = \sqrt{\int |x|^2 d\omega}$, is used to assess the performance of the algorithm and to adapt the stepsize so that δ_{RLE} is kept

within a target range ($\delta_G/2, \delta_G$), specified by a goal local error δ_G provided by the user. Let us note that in order to advance a solution by one z -slice of extend Δz , the local-error method performs possibly multiple substeps of extend $h \leq \Delta z$. The protocol for adapting the local step size h distinguishes three cases [26]:

1. If $\delta_{\text{RLE}} > 2\delta_G$, discard the current trial solution $\mathcal{E}_\omega(z+h)$ and retry the substep with $h \leftarrow h/2$.
2. If $\delta_G < \delta_{\text{RLE}} \leq 2\delta_G$, keep the trial solution and decrease the stepsize to $h \leftarrow 2^{-1/3}h$ for the next substep.
3. If $\delta_{\text{RLE}} < \delta_G/2$, keep the trial solution and increase the stepsize to $h \leftarrow 2^{1/3}h$ for the next substep.

Otherwise, if the relative local error is within the target range specified by the goal local error, the trial solution and local stepsize are kept. The substep completing each z -slice is truncated to terminate exactly at $z + \Delta z$. Thus, on termination of the algorithm, the field solution \mathcal{E}_ω is available on a discrete z -grid with constant spacing Δz . By default, the LEM algorithm is used in conjunction with a RK2 z -stepping formula. A solver based on the above procedure is implemented as LEM (in the text referred to as LEM).

4.6. Conservation quantity error method (CQE)

We here also provide an implementation of the conservation quantity error (CQE) method [27], wherein stepsize adaption is controlled by a conservation law of the underlying model equation. To advance a solution from position z to $z+h$, the integrating factor method IFM-RK4IP (sect. 4.4) is used. By default, Eq. (11) is used to guide stepsize adaption. For this purpose, the relative photon number error [27]

$$\delta_{\text{Ph}}(z) = \frac{|C_p(z+h) - C_p(z)|}{C_p(z)} \quad (23)$$

is monitored and compared to a user provided goal local error δ_G . In terms of the CQE, the protocol for adapting the stepsize h reads [27]:

1. If $\delta_{\text{Ph}} > 2\delta_G$, discard the current trial solution $\mathcal{E}_\omega(z+h)$ and retry the substep with $h \leftarrow h/2$.
2. If $\delta_G < \delta_{\text{Ph}} \leq 2\delta_G$, keep the trial solution and decrease the stepsize to $h \leftarrow 2^{-1/5}h$ for the next substep.
3. If $\delta_{\text{Ph}} < 0.1\delta_G$, keep the trial solution and increase the stepsize to $h \leftarrow 2^{1/5}h$ for the next substep.

Otherwise, if the relative local error is within the target range ($0.1\delta_G, \delta_G$), specified by the goal local error, the trial solution and local stepsize are kept. A solver based on the above procedure, valid in the no-loss limit ($\alpha = 0$), is implemented as CQE. The conservation law used to control stepsize adaption can be changed by the user by providing a suitable function when an instance of the solver is initialized. An example is provided [online](#) in the extended user guide [13].

5. User manual

Below we clarify the structure of the `py-fmas` python package and detail a typical workflow involving the `py-fmas` package. Usage examples that employ the `py-fmas` library code are discussed in sect. 9.

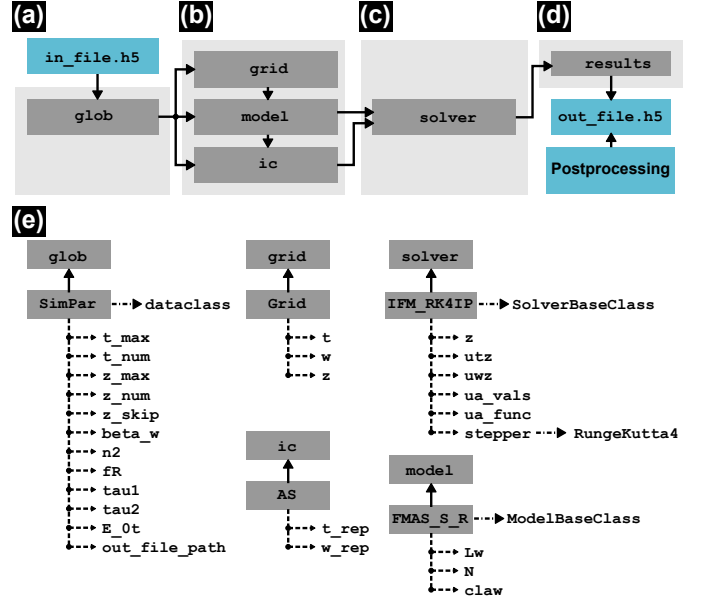


Fig. 1. (a-d) Pictorial outline of a workflow using the `py-fmas` library code. (a) Specification of a full simulation run. (b) Initialization of the model. (c) Initialization of the propagation scheme and z -propagation. (d) Data storage. Input data, output data and postprocessing tools are part of more “specific project” code. (e) Relationships between selected objects relevant to the minimal example in listing 1. In (e), solid arrows indicate class instantiation (“creates” relationship), dashed arrows indicate attributes and methods (“has-a” relationship), dash-dotted arrow indicates reference to an object (“is-a” relationship).

5.1. Structure of the `py-fmas` package

`py-fmas` is a pure Python package, organized as a collection of modules. The scope and capabilities of the individual modules are summarized below. Further information is available in the [online reference manual](#) [13].

- `models`: Subpackage implementing the propagation models for the analytic signal discussed in sect. 2 (see Tab. 1). Also provides a data structure allowing to implement custom models.
- `solver`: Subpackage implementing the z -propagation algorithms detailed in sect. 4. Also provides a data structure allowing to implement custom algorithms.
- `propagation_constant`: Provides several propagation constants. Also provides a data structure for analyzing user-defined propagation constants (Appendix D).
- `raman_response`: Provides functions that implement several Raman response models (Appendix C).
- `stepper`: Provides the z -stepping formulas used by the propagation algorithms (sect. 4.1).
- `analytic_signal`: Provides data structures for converting discrete-time optical field to discrete time analytic signal.
- `data_io`: Provides functions and data structures for reading and writing data in HDF5-format.

- `tools`: Provides functions for postprocessing (see [Appendix B](#)) and visualizing simulation data, as well as functions that did not fit into the other modules.
- `config`: Module containing functions and parameters jointly used by several modules.

5.2. Availability of the software

`py-fmas` is openly available [13], hosted on the code development platform `gitHub` (<https://github.com>). It is implemented in Python3 under the MIT license. The software can be installed by cloning the repository and installing the provided Python3 wheel:

```
> git clone https://github.com/omelchert/py-fmas.git
> cd ./py-fmas/dist
> python3 -m pip install ./py_fmas-1.0-py3-none-any.whl
```

5.3. Specifying a propagation scenario

While our computational research projects are usually carried out by scripting, incorporating `py-fmas` library code into more specific project code as needed, we also provide convenience methods that allow a user to read a propagation scenario from an input file in HDF5-format [Fig. 1(a)]. This file must contain all necessary simulation parameters for specifying the computational domain, propagation model, and, propagation algorithm. All required parameters are listed in Tab. 3. Let `in_file.h5` be an adequate input file, then a workflow can be started by importing the `fmas` package (listing 1, line 1), and reading the simulation parameters using the function `read_h5()` contained in module `data_io` (listing 1, line 3). The obtained data structure `glob` is an instance of the dataclass `SimPars`, implemented in `data_io` as well. The various parameters held by `SimPars` [Fig. 1(e)] are detailed in Tab. 3 in [Appendix A](#). This completes the first stage of the workflow outlined in Fig. 1(a). Let us note that the minimal example in listing 1 does not use all of all the parameters implemented by the dataclass. A more general application-type example that does this is discuss in sect. 5.7 below. An example, demonstrating how to generate an adequate input file, is provided along with the [online documentation](#) [13].

5.4. Initializing a model

Once a propagation scenario is specified, the problem specific data structures can be initialized [Fig. 1(b)]. First, a computational grid, called `grid`, is obtained as instance of the class `Grid` (listing 1, lines 5–9). `Grid` provides attributes for convenient access to the discrete coordinate axes [Fig. 1(e)]. For example, `grid.t` returns a `numpy.ndarray` of length $M = t_{\text{num}}$, defining the temporal grid points

$$t_m = -t_{\text{max}} + m \Delta t, \quad m = 0, \dots, M - 1, \quad (24a)$$

with $\Delta t = 2t_{\text{max}}/t_{\text{num}}$ available as `grid.dt`. Likewise, `grid.w` returns an array containing the angular frequency grid points in standard order [30, 17], i.e.

$$\omega_m = \begin{cases} m \Delta \omega, & \text{for } m = 0, \dots, \frac{M}{2} - 1, \\ (m - M) \Delta \omega, & \text{for } m = \frac{M}{2}, \dots, M - 1, \end{cases} \quad (24b)$$

with $\Delta \omega = \pi/t_{\text{max}}$ available as `grid.dw`, and `grid.z` returns an array of length $z_{\text{num}} + 1$, containing the grid points

$$z_n = 0 + n \Delta z, \quad n = 0, \dots, z_{\text{num}}, \quad (24c)$$

along the propagation axis z , where the extend of a single z -slice $\Delta z = z_{\text{max}}/z_{\text{num}}$ is available as `grid.dz`.

Next, one of the propagation models implemented in module `models`, namely the simplified forward model including the Raman effect (FMAS_S_R), is initialized [listing 1, lines 11–17; Fig. 1(e)], and the initial condition $E_0(t_m)$, $m = 0, \dots, M - 1$, is used to initialize a data structure holding the corresponding discrete-time analytic signal [listing 1, line 19; Fig. 1(e)].

Listing 1: Exemplary workflow using the `py-fmas` library code.

```
1 import fmas
2
3 glob = fmas.data_io.read_h5('in_file.h5')
4
5 grid = fmas.grid.Grid(
6     t_max = glob.t_max,
7     t_num = glob.t_num,
8     z_max = glob.z_max,
9     z_num = glob.z_num)
10
11 model = fmas.models.FMAS_S_R(
12     w = grid.w,
13     beta_w = glob.beta_w,
14     n2 = glob.n2,
15     fR = glob.fR,
16     tau1 = glob.tau1,
17     tau2 = glob.tau2)
18
19 ic = fmas.analytic_signal.AS(glob.E_0t)
20
21 solver = fmas.solver.IFM_RK4IP(
22     model.Lw, model.Nw,
23     user_action = model.claw)
24 solver.set_initial_condition(
25     grid.w, ic.w_rep)
26 solver.propagate(
27     z_range = glob.z_max,
28     n_steps = glob.z_num,
29     n_skip = glob.z_skip)
30
31 res = {
32     "t": grid.t,
33     "z": solver.z,
34     "w": solver.w,
35     "AS_tz": solver.utz,
36     "Cp": solver.ua_vals}
37 fmas.data_io.save_h5('out_file.h5', **res)
```

5.5. Initializing a solver and running a simulation

Now that computational grid, model, and initial condition are set up, a specific z -propagation algorithm can be initialized [Fig. 1(c)]. In lines 21ff, the minimal example in listing 1 shows how to initialize an instance of the IFM-RK4IP solver [Fig. 1(e)], implemented in module `solver`. In line 22, the frequency-domain representation of the linear and nonlinear operators are handed over. In line 23, an additional user-specified callback function is initialized, that will be evaluated at each z -step. Internally it is assigned to the class method `ua_fun`. If a callback function is provided it needs to exhibit an interface of the form `my_fun(idx, zcurr, w, uw)`, where `idx` (type `int`) labels the current z -position `zcurr` (type `float`), `w` is the angular frequency grid (type `numpy.ndarray`), and `uw` is the frequency domain representation of the field at the current z -position (type `numpy.ndarray`). Here, `model.claw` is handed

over as callback function. For the model specified in line 11, the method `claw` implements the conserved quantity Eq. (11).

In line 24f, the initial condition is set. Let us note that all z -propagation algorithms implemented in `fmas` predominantly work in the frequency domain. Hence, when setting the initial condition for the solver, a design decision was to hand over the frequency-domain representation of the discrete-time analytic signal. In the second argument of the method call `set_initial_condition` this is achieved by `ic.w_rep`, which implements the frequency-domain algorithm [28]

$$\mathcal{E}_{\omega_m} = \begin{cases} E_{\omega_m}, & m = 0, \\ 2E_{\omega_m}, & 1 \leq m \leq M/2 - 1, \\ E_{\omega_{M/2}}, & m = M/2, \\ 0, & M/2 + 1 \leq m \leq M - 1, \end{cases} \quad (25)$$

computing the frequency-domain representation of the discrete-time analytic signal (\mathcal{E}_{ω_m} , $m = 0, \dots, M - 1$), based on the frequency-domain representation of the real optical field (E_{ω_m} , $m = 0, \dots, M - 1$). A simulation run is best started with “consistent” initial conditions that satisfy the boundary condition Eq. (12b). For example, for a propagation scenario starting off from a localized field pulse $\mathcal{E}_0(t)$, the extend $T = 2t_{\max}$ of the periodic time domain should be set large enough so that $|\mathcal{E}_0(\pm t_{\max})| \approx 0$.

In lines 26–29 the algorithm is started, at which point the propagation range (`z_range`) and number of integration steps (`z_steps`) are specified. The additional parameter `n_skip` specifies the number of z -steps that are skipped in between two stored field configurations. This allows the user to reduce the amount of output data generated by the solver. While executing, the solver will evaluate the right-hand-side terms of Eq. (13) to perform the numerical integration along the z -grid and it will evaluate the optional user-specified callback-function, if this is scheduled as shown in line 23. The generated data will be stored on a discrete grid with grid points $z'_n = n \Delta z'$, with $\Delta z' = z_{\max}/N'$, where $n = 0, \dots, N'$ and $N' = z_{\text{num}}/z_{\text{skip}}$.

Once the algorithm terminates, the time-domain representation of the discrete-time analytic signal, given by $\mathcal{E}(z'_n, t_m)$, with $n = 0, \dots, N'$, and $m = 0, \dots, M - 1$, is available as a two-dimensional `numpy.ndarray` retrieved by calling `solver.utz`. Likewise, $\mathcal{E}_{\omega_m}(z'_n)$, $n = 0, \dots, N'$, $m = 0, \dots, M - 1$, can be retrieved by calling `solver.uwz`. The conserved quantity $C_p(z'_n)$, with $n = 0, \dots, N'$, is available as one-dimensional `numpy.ndarray` upon calling `solver.ua_vals`. Finally, the reduced z -grid with grid points z'_n , $n = 0, \dots, N'$, is available as one-dimensional `numpy.ndarray` upon calling `solver.z`. Let us note that `solver.z` and `grid.z` have the same length only for `n_skip = 1`. Subsequently, we will refer to the coordinates z' , at which a field solution is given, simply as z .

5.6. Data storage

After the z -propagation algorithm has terminated, the generated data can be saved to an output file in HDF5-format [Fig. 1(d)]. For this purpose, we set up a dictionary containing

a `key:data-pair` with custom key for each data object we want to save (lines 31–36), and pass it to function `save_h5` provided by module `data_io` (line 37).

5.7. Using fmas as application

The `py-fmas` package can also be used as an application which interprets all the attributes implemented by the dataclass `SimPars`, see Fig. 1(e) and Tab. 3. Such functionality is implemented by the function `run` in module `app`. A minimal interactive python session that uses the `fmas` library code as an app reads:

```
>>> import fmas
>>> fmas.run('in_file.h5')
```

A step-by-step example, demonstrating how to use `py-fmas` as a black-box application, choose a specific propagation model and algorithm, save data, and generate a simple figure of the output is provided along with the [online documentation](#) [13].

5.8. Data postprocessing

For subsequent analysis it is useful to consider the transformed field $\mathcal{E}'_{\omega}(z) = \mathcal{E}_{\omega}(z) \exp(i\omega z/v_0)$, shifted to a moving frame of reference. The time-domain representation $\mathcal{E}'(z, t)$ then corresponds to the analytic signal $\mathcal{E}(z, \tau)$ for the retarded time $\tau = t - z/v_0$. The reference velocity v_0 can be chosen so that the time-domain dynamics appears slow. For changing the frame of reference in this way, module `tools` provides a function with interface

```
change_reference_frame(w, z, uwz, v0)
```

where `w` (type `numpy.ndarray`) is the ω -grid, `z` (type `numpy.ndarray`) is the z' -grid, `uwz` (type `numpy.ndarray`) is the two-dimensional frequency-domain representation of the analytic signal $\mathcal{E}_{\omega}(z)$, and `v0` (type `float`) is the reference velocity v_0 .

Generally, generation of input data, postprocessing of output data and data visualization is part of more specific project code and is not covered by the minimal example discussed above. However, in module `tools`, `py-fmas` features simple functions that assist a user to quickly visualize the generated data. As demonstrated in sect. 9.3, `py-fmas` also includes the functionality to compute simple spectrograms.

6. Software dependencies

`py-fmas` is provided as a Python3 package [29]. It uses a wide range of standard-library Python packages. The dependencies of `py-fmas` include:

- The Numpy and Scipy packages for python [30, 31].
- The Matplotlib for data visualization [32].
- The HDF5 C-library for reading and writing files in HDF5 format, and its Python wrapper `h5py` [33, 34].

7. Software documentation

py-fmas is openly available. The online documentation includes a reference manual with details on the implemented models and propagation algorithms, an extended user guide with step-by-step demonstrations of the functionality of py-fmas, and further usage examples. Links to the code-repository and the documentation are available under <https://github.com/omelchert/py-fmas> [13].

8. Software extensibility

py-fmas is based on our research code and was implemented with the aim of being easily extendible and maintainable. For example, by using the base class `ModelBaseClass`, contained in module `models`, it is straight-forward to implement further z -propagation models for use with the py-fmas library code. An example that shows how an envelope model, given by the usual nonlinear Schrödinger equation (used in sect. 9.1), can be set up is provided along with the [online documentation](#) [13]. There, we also demonstrate how to extend py-fmas by models implementing the Korteweg-deVries equation [35] and the Lugiato-Lefever equation [36, 37]. In addition, we show how the provided software can be used to simulate backscattered components of the optical field in terms of a bidirectional model for a complex field [6]. While this lies well within the capabilities of the provided software, it is outside the intended application domain of py-fmas. Further z -propagation schemes can be implemented via the `SolverBaseClass` provided in module `solver`. For example, implementing the “Embedded Runge-Kutta scheme for step-size control in the interaction picture method” (ERK4(3)-IP) [38, 39], for use with analytic signal based models, is directly possible. Another possibility is to extend the functionality of py-fmas by the `optfrog` Python package [40], allowing to compute analytic signal spectrograms with optimized time and frequency resolution. An example that illustrates this is available [online](#) [13].

9. Usage examples

Below we show three use-cases of the software. In sect. 9.1 we demonstrate the accuracy of the implemented algorithms when applied to the single soliton problem of the standard nonlinear Schrödinger equation (NSE) [41, 18, 20], i.e. a test-case for which an exact solution is available. In sect. 9.2 we reproduce an exemplary simulation of supercontinuum generation in a photonic crystal fiber (PCF) [42, 43, 44, 25, 27], and compare the performance of fixed and adaptive stepsize schemes. In sect. 9.3 we show a complex propagation scenario involving multiple interacting pulses at different center frequencies, out of the range of the generalized nonlinear Schrödinger equation (GNSE).

9.1. Exact single-soliton solution of the NSE

We first demonstrate that the functionality of the software can be extended by implementing additional models. Specifically, we here consider an envelope model given by the usual

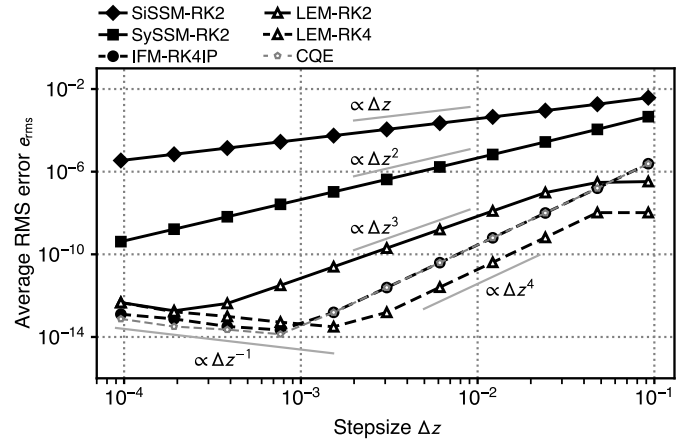


Fig. 2. Average root-mean square (RMS) error of the different propagation schemes as function of the stepsize Δz . Data is shown for different solver types (SiSSM: Simple split-step Fourier method; SySSM: Symmetric split-step Fourier method; IFM-RK4IP: Variant of integrating factor method aka. “Runge-Kutta in the interaction picture” method; LEM: Local error method; CQE: Conservation quantity error method) and z -stepping formulas (RK2: second-order Runge-Kutta formula, solid lines; RK4: fourth-order Runge-Kutta formula, dashed lines).

nonlinear Schrödinger equation in the form [5, 41]

$$\partial_z A = i \frac{1}{2} \partial_t^2 A + i |A|^2 A, \quad (26)$$

for the slowly varying complex pulse amplitude $A \equiv A(z, t)$, where, for clarity, z and t are treated as dimensionless coordinates. The exact single-soliton solution of Eq. (26) [41, 45, 4], for unit pulse-width given by

$$A_{\text{sol}}(z, t) = \text{sech}(t) e^{-iz/2}, \quad (27)$$

offers a possibility to assess the accuracy of the implemented z -stepping algorithms. Subsequently, we consider Eq. (26) with initial condition $A(0, t) = \text{sech}(t)$. For the computational domain we choose $t_{\text{max}} = 40$, $t_{\text{num}} = 4096$, and propagate for one soliton period, i.e. up to $z_{\text{max}} = \pi/2$, using different step sizes Δz . Although the NSE allows for more specific implementations of split-step Fourier methods that rely on an exact solution of the nonlinear subproblem, we here opt to solve Eq. (26) using the algorithms specified in sect. 4. In Fig. 2 we show the resulting average root-mean square error (rms-error)

$$e_{\text{rms}} = \sqrt{\langle |A(z_{\text{max}}, t) - A_{\text{sol}}(z_{\text{max}}, t)|^2 \rangle} \quad (28)$$

at the final z -position as function of Δz . In Eq. (28), $A(z, t)$ specifies the result of the numerical integration at a given step size Δz . For all propagation schemes, a scaling behavior $e_{\text{rms}}(\Delta z) = C \Delta z^r$, for $\Delta z > 10^{-3}$ is clearly evident (r denotes the scaling order of the rms-error, see Fig. 2). We find the expected scaling of the global error for the different propagation algorithms down to a saturation at $e_{\text{rms}} \approx 10^{-13}$. As evident from Fig. 2, for this test problem, the local error method (LEM) with a RK4 z -stepping formula exceeds the naively expected $O(\Delta z^3)$ behaviour by achieving an effective scaling $O(\Delta z^4)$, a fortunate fact previously also noted in Ref. [27]. Using a RK2 formula

for z -stepping yields the expected $O(\Delta z^3)$ error bound. For very small values of Δz , the scaling behavior for the IFM and LEM algorithms is $\propto \Delta z^{-1}$, i.e. proportional to the number of performed Fourier-transforms. Since Δz is small, this implies an overall large number of additions and multiplications. Consequently, the error scaling is dominated by the accumulated round-off error.

While the NSE provides a valuable testbed for assessing the performance of the implemented algorithms, its ability to describe the dynamical evolution of spectrally broad, ultrashort optical pulses is limited [3, 11, 16]

9.2. Supercontinuum generation in a PCF

Next, we reproduce numerical results of a supercontinuum generation process in a photonic crystal fiber (PCF). The underlying propagation scenario is discussed on several occasions in the scientific literature [44, 25, 27]. For example, in Ref. [44], it is used to demonstrate numerical simulations in terms of the generalized nonlinear Schrödinger equation (GNSE) using the split-step Fourier method. In Ref. [25] it is used to introduce the ‘‘Runge-Kutta in the interaction picture’’ (RK4IP) method (sect. 4.4). In Ref. [27] it is used to demonstrate the feasibility of the conservation quantity error method (CQE; sect. 4.6) for the simulation of supercontinuum generation in optical fibers. To investigate the sensitivity of the supercontinuum generation process on different kinds of instabilities, an eighth-order Runge-Kutta scheme with adaptive stepsize control has been used to ensure a high accuracy [42, 43]. All the above simulation studies used the GNSE, which relies on the slowly varying envelope approximation. In contrast to this, we here employ also a non-envelope model given by the simplified forward model for the analytic signal with added Raman effect (FMAS-S-R). Specifically, we consider Eq. (9) with a polynomial approximation of the propagation constant, given by

$$\beta(\omega) = \sum_{n=2}^{10} \frac{\beta_n}{n!} (\omega - \omega_0)^n, \quad (29)$$

with parameters β_n listed in Tab. 2, $\omega_0 = \text{rad/fs}$ and $n_2 = \gamma c/\omega_0$ with $\gamma = 0.11 \cdot 10^{-6} \text{ W}^{-1} \text{ m}^{-1}$. The frequency dependence of the relative group delay $\beta_1(\omega) = \partial_\omega \beta(\omega)$ [note that using Eq. (29) $\beta_1(\omega_0) = 0 \text{ fs}/\mu\text{m}$], and group-velocity dispersion $\beta_2(\omega) = \partial_\omega^2 \beta(\omega)$ are shown in Fig. 3(a). The parameters specifying the Raman effect are set to $f_R = 0.18$, $\tau_1 = 12.2 \text{ fs}$, and

Table 2

Expansion coefficients β_n (in units of $\text{fs}^n/\mu\text{m}$) for the polynomial approximation of the propagation constant in Eq. (29). Values are derived from the data shown in Tab. 1 of Ref. [44].

n	$\beta_n \left(\frac{\text{fs}^n}{\mu\text{m}} \right)$	n	$\beta_n \left(\frac{\text{fs}^n}{\mu\text{m}} \right)$	n	$\beta_n \left(\frac{\text{fs}^n}{\mu\text{m}} \right)$
2	-0.011 830	5	0.207 37	8	-2.5495
3	0.081 038	6	-0.539 43	9	3.0524
4	-0.095 205	7	1.348 60	10	-1.7140

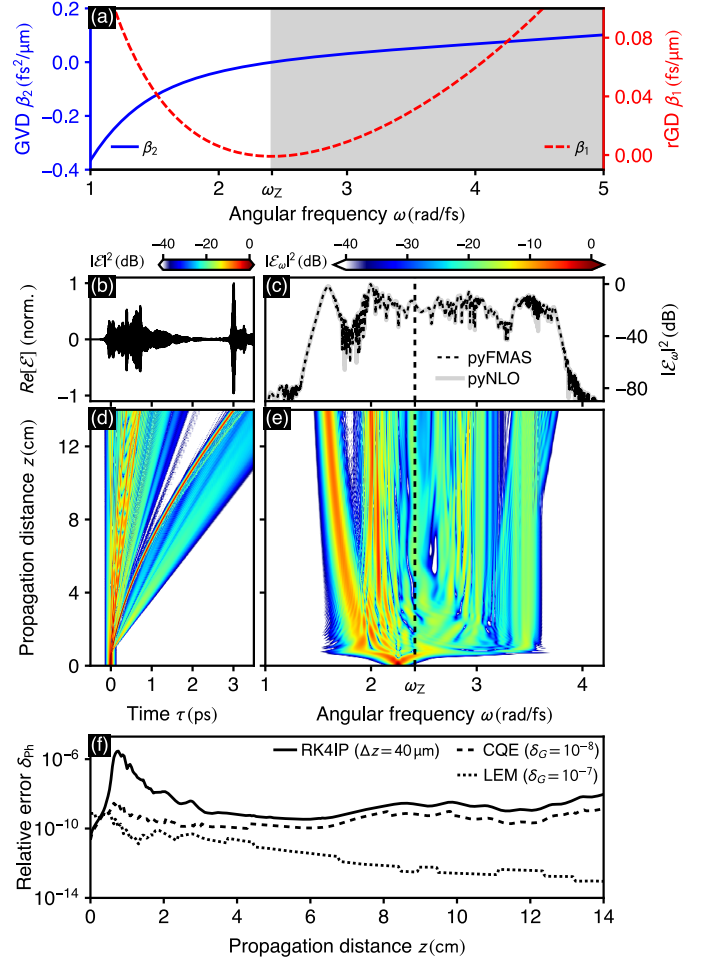


Fig. 3. Exemplary simulation of supercontinuum generation in a PCF. (a) Frequency dependence of the relative group-delay (rGD) $\beta_1(\omega)$, and group-velocity dispersion (GVD) $\beta_2(\omega)$. Shaded region indicates domain of normal dispersion with zero dispersion point $\omega_z \approx 2.415$ rad/fs. (b) Optical field $E = \text{Re}[E]$ at $z = 14$ cm. (c) Spectrum $|\mathcal{E}_\omega|^2$ at $z = 14$ cm. Solid line indicates results obtained using pyNLO [46]. Dashed line shows results obtained using py-fmas IFM-RK4IP solver with stepsize $\Delta z = 40 \mu\text{m}$. Evolution of (d) intensity, and, (e) spectrum over the length of the PCF. Vertical dashed line in (c,e) indicates zero-dispersion point. (f) Relative photon number error δ_{ph} obtained for the IFM-RK4IP solver, the local error method (LEM) and the conservation quantity error method (CQE).

$\tau_2 = 32$ fs. As initial condition we use

$$E(0, t) = \text{Re} \left[\sqrt{P_0} \text{sech}(t/t_0) e^{-i\omega_0 t} \right], \quad (30)$$

with $P_0 = 10 \text{ kW}$, and $t_0 = 28.4 \text{ fs}$. For the computational domain we choose $t_{\text{max}} = 3.5 \text{ ps}$, $t_{\text{num}} = 2^{14}$, and propagate up to $z_{\text{max}} = 14 \text{ cm}$ using step size $\Delta z = 40 \mu\text{m}$. For z -propagation we use the IFM-RK4IP method. The propagation dynamics of the field in both, time domain and frequency domain, is detailed in Figs. 3(b-e). In Fig. 3(b,d), the pulse dynamics is shown as function of the retarded time $\tau = t - \beta_1(\omega_0)z$. In Fig. 3(c) we compare the analytic signal spectrum $|\mathcal{E}_\omega|^2$ at $z = 14 \text{ cm}$ to results obtained using the pyNLO code [46]. Both agree well on a qualitative basis. Figure 3(f) shows the relative photon number error defined in Ref. [27], related to the conserved quantity in Eq. (11) through $\delta_{\text{ph}}(z) = |C_p(z + \Delta z) - C_p(z)|/C_p(z)$. For

the simulation run with stepsize $\Delta z = 40 \mu\text{m}$, the maximum photon number error is $\delta_{\text{ph}} \approx 2.9 \cdot 10^{-6}$ at $z \approx 0.76 \text{ cm}$ [see Fig. 3(f)]. We can compare this to the results shown in Fig. 1(d) of Ref. [27], exhibiting the somewhat larger peak photon error of $\delta_{\text{ph}} \approx 6 \cdot 10^{-6}$. In Fig. 3(f) we also included the relative photon number error obtained from a simulation run using the local error method (LEM), with local goal error set to $\delta_G = 10^{-7}$, and the conservation quantity error method (CQE; $\delta_G = 10^{-8}$). Here, the advantage of the adaptive stepsize schemes is clearly evident. During the early propagation stage, i.e. for $z < 2 \text{ cm}$, a decreased stepsize prevents the pronounced peak of the relative photon number error exhibited by the fixed stepsize algorithm.

Let us note that an adequate representation of the material dispersion for simulating the propagation dynamics of ultrashort optical pulses is critical for obtaining accurate numerical results [47, 11]. Thus, for simulations in the few-cycle regime, a truncated Taylor expansion of the propagation constant, such as Eq. (29), in conjunction with a highly accurate propagation algorithm can be counterproductive.

9.3. Interaction of four pulses in a ESM fiber

Finally, we consider a complex scenario, involving the simultaneous propagation of multiple pulses with distinct center frequencies. In particular, we consider the medium properties of an “endlessly single mode” (ESM) nonlinear photonic crystal fiber [48], which we implement by a rational Padé-approximant of order $[N = 8/M = 8]$ for the medium refractive index in the form

$$n(\omega) = 1 + \frac{\sum_{n=0}^N p_n \omega^n}{1 + \sum_{m=1}^M q_m \omega^m}. \quad (31)$$

The parameter sequences $\{p_n\}_{n=0}^N$ and $\{q_m\}_{m=1}^M$ are detailed in Appendix D, where a convenience class for handling propagation constants is introduced. Representing the medium dispersion as in Eq. (31) has several advantages [49, 50]. It gives a better approximation of the refractive index than truncating a Taylor expansion for the detuning $\omega - \omega_0$ for some reference frequency ω_0 , avoids rapid divergence for large frequencies, and, in particular, helps to avoid unnecessary numerical stiffness when solving nonlinear propagation equations.

The resulting profiles of the group-delay $\beta_1(\omega)$ and group-velocity dispersion $\beta_2(\omega)$ are shown in Fig. 4(a). For the simulation in terms of the FMAS-S Eq. (8) we set $n_2 = 3 \cdot 10^{-8} \mu\text{m}^2\text{W}^{-1}$ and neglect the Raman effect. As initial condition, we consider a fundamental soliton, given by

$$E_S(0, t) = \text{Re} \left[A_0 \text{sech}(t/t_S) e^{-i\omega_S t} \right], \quad (32)$$

with amplitude $A_0 = \sqrt{|\beta_2(\omega_S)|c/(n_2\omega_S t_S^2)}$ and parameters $(t_S, \omega_S) = (20 \text{ fs}, 1.5 \text{ rad/fs})$. We further consider a train of three dispersive waves in the form

$$E_{\text{DW}}(0, t) = \sum_{n=1}^3 \text{Re} \left[A_{\text{DW}} \text{sech} \left(\frac{t - \delta_n}{t_{\text{DW}}} \right) e^{-i\omega_n t} \right], \quad (33)$$

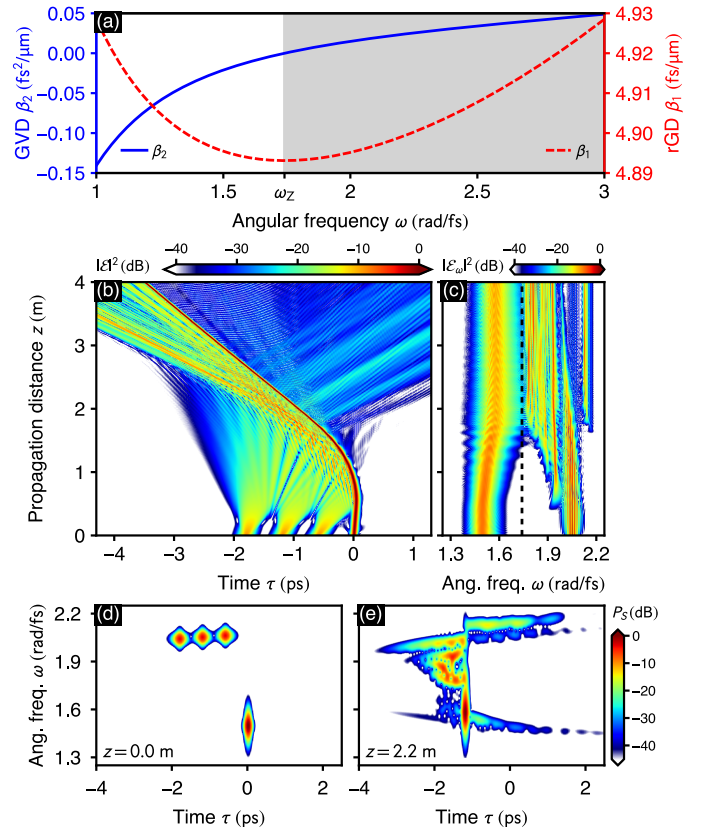


Fig. 4. Four pulse interaction in an ESM photonic crystal fiber (PCF). (a) Frequency dependence of the group-delay (GD) $\beta_1(\omega)$, and group-velocity dispersion (GVD) $\beta_2(\omega)$. Shaded region indicates domain of normal dispersion with zero dispersion point $\omega_Z \approx 1.741 \text{ rad/fs}$. Evolution of (b) intensity, and, (c) spectrum over the length of the PCF. Vertical dashed line in (c) indicates zero-dispersion point. (d) Spectrogram at $z = 0 \text{ m}$, and (e) spectrogram at $z = 2.2 \text{ m}$.

with common amplitude $A_{\text{DW}} = 0.35 A_0$, common duration $t_{\text{DW}} = 60 \text{ fs}$, and parameters $(\delta_1, \omega_1) = (-0.6 \text{ ps}, 2.06 \text{ rad/fs})$, $(\delta_2, \omega_2) = (-1.2 \text{ ps}, 2.05 \text{ rad/fs})$, and $(\delta_3, \omega_3) = (-1.8 \text{ ps}, 2.04 \text{ rad/fs})$. For the computational domain we choose $t_{\text{max}} = 8 \text{ ps}$, $t_{\text{num}} = 2^{15}$, and propagate up to $z_{\text{max}} = 6 \text{ m}$ using step size $\Delta z = 80 \mu\text{m}$. For z -propagation we use the IFM-RK4IP method. The propagation dynamics of the field in both, time domain and frequency domain, is detailed in Figs. 4(b-c). Specifically, Fig. 4(b) shows the time-domain intensity of the analytic signal for the retarded time coordinate $\tau = t - z/v_0$, with reference velocity $v_0 = 1/\beta_1(\omega_S)$. As evident from the spectrogram (see Appendix B) in Fig. 4(d), all four pulses can be distinguished very well for the initial condition at $z = 0 \text{ m}$. Upon propagation, a complex dynamics unfolds as can be seen from Figs. 4(b-c) and the spectrogram at $z = 2.2 \text{ m}$ [Fig. 4(e)]. Therein, the soliton induces a strong refractive index barrier for the dispersive waves in the domain of normal dispersion [51], leading to multiple scattering processes. The underlying process is enabled by a general wave reflection mechanism, originally reported in fluid dynamics [52]. In optics it is referred to as the push-broom effect [53], optical event horizon [54, 55], or temporal reflection [56]. It allows for a strong and efficient all optical control of light by light

Table 3

Simulation parameters used to specify a propagation scenario. These are all the recognized parameters to be found in the parameter input file. Parameters with default setting are optional.

Parameter	Symbol	Value type	Description	Unit
<code>t_max</code>	t_{\max}	float	Half-period of temporal mesh	fs
<code>t_num</code>	t_{num}	int	Number of mesh points in t	–
<code>z_max</code>	z_{\max}	float	Value of last mesh-point along z	μm
<code>z_num</code>	z_{num}	int	Number of z -slices, i.e. z -steps, along z	–
<code>z_skip</code>	z_{skip}	int	Step-interval in which data is stored upon z -propagation (default: 1) Example: for $z_{\text{skip}} = 4$, data is stored at every 4th integration step	–
<code>beta_w</code>	$\beta(\omega)$	numpy.ndarray	Propagation constant	rad/fs
<code>n2</code>	n_2	float	Nonlinear refractive index	$\mu\text{m}^2/\text{W}$
<code>fR</code>	f_R	float	Fractional contribution of Raman response	–
<code>tau1</code>	τ_2	float	Raman response time scale	fs
<code>tau2</code>	τ_1	float	Raman response time scale	fs
<code>E_0t</code>	$E(0, t)$	numpy.ndarray	Real-valued optical field at $z = z_{\min}$	\sqrt{W}
<code>out_file_path</code>	–	str	Full path for output file (default: <code>results.dat</code>)	–

[57, 58], and has been shown to naturally appear in the process of supercontinuum generation [59, 60, 9, 61].

The above propagation scenario illustrates the simulation of complex short-pulse interaction dynamics, as, e.g., given in all-optical supercontinuum switching [62]. The simulations in Ref. [62] were performed using the `py-fmas` library code.

Appendix A. Recognized input-file parameters

As discussed in sect. 5.3, `py-fmas` provides convenience methods that read a user-defined propagation scenario from an adequate input file in HDF5 format. In that case, the input file must contain all parameters needed to specify the computational domain, propagation model, and propagation algorithm. In Tab. 3 we list the recognized parameters that can be supplied in terms of such an input file. All parameters without default values must be present.

Appendix B. Computing spectrograms

A spectrogram provides a particular time-frequency representation of a considered signal and represents an integral tool in the analysis and characterization of ultrashort optical pulses, both in theory [63, 64] and experiment [65, 66, 67]. `py-fmas` includes the functionality to compute a spectrogram of the time-domain analytic signal $\mathcal{E}(z, t)$ at a given z -coordinate in terms of a short-time Fourier transform as

$$P_S(t, \omega) = \frac{1}{2\pi} \left| \int \mathcal{E}(z, t') h(t' - t) e^{-i\omega t} dt' \right|^2, \quad (\text{B.1})$$

wherein $h(x) = \exp(-x^2/2\sigma^2)$ specifies a Gaussian window function with root-mean-square width σ , used to localize $\mathcal{E}(z, t)$ in time. For computing such spectrograms, module `tools` provides the function

`spectrogram(t, w, ut, t_lim, Nt, Nw, s0)`

where `t` (type `numpy.ndarray`) is the t -grid Eq. (24a), `w` (type `numpy.ndarray`) is the ω -grid Eq. (24b), `ut` (type `numpy.ndarray`) is the analytic signal $\mathcal{E}(z, t)$ at a given z -coordinate, `t_lim` (type `list`) is a 2-tuple specifying bounds for the t -axis when computing the spectrogram (default: `(min(t), max(t))`), `Nt` (type `int`) is the number of equidistant samples used for localization along t (default: 1000), `Nw` (type `int`) is the number of equidistant ω -samples kept on output (default: 2^8), and `s0` (type `float`) is the RMS width of h in Eq. (B.1) (default: 20 fs). Upon termination, the above function returns the 3-tuple `(tS, wS, PS)`, with `tS` (type `numpy.ndarray`), and `wS` (type `numpy.ndarray`) the spectrograms discrete t and ω axes, and `PS` (type `numpy.ndarray`) the corresponding two-dimensional spectrogram trace. A function with call-signature `plot_spectrogram(tS, wS, PS)`, assisting a user to quickly visualize the spectrogram data, is also included in module `tools`.

Note that `py-fmas` can also be used in conjunction with the `optfrog` spectrogram tool [40], allowing a user to calculate spectrograms with optimized time-frequency resolution. Examples that illustrate how to use the above functions as well as how to blend `py-fmas` with `optfrog` are provided along with the [online documentation](#).

Appendix C. Raman response functions

Numerical models of the Raman response are important for the accurate theoretical description of the propagation of optical pulses with short duration and high peak power [68, 69]. For example, the Raman response includes the self-frequency shift that affects the propagation dynamics of solitons. `py-fmas` implements several models of the Raman response function, located in module `raman_response`. Specifically, the implemented models are:

- Blow-Wood type response function [14]: The time-domain formulation of this response function, based on a single-damped-harmonic-oscillator approximation with

Lorentzian linewidth, reads

$$h_{\text{BW}}(t) = \frac{\tau_1^2 + \tau_2^2}{\tau_1 \tau_2} e^{-t/\tau_2} \sin(t/\tau_1) \theta(t), \quad (\text{C.1})$$

where causality is assured by the unit step function $\theta(t)$. Equation (C.1) represents a generic two parameter response function that can be adapted to fit various types of nonlinear fibers. For example, using a fractional Raman contribution $f_R = 0.18$ [cf. Eq. (9)] together with $\tau_1 = 12.2$ fs, and $\tau_2 = 32$ fs is adequate for simulation of silica fibers [14]. Using $f_R = 0.1929$, $\tau_1 = 9$ fs, and $\tau_2 = 134$ fs is adequate for ZBLAN fluoride fibers [70, 71]. This response model is implemented as function `h_BW(t, tau1, tau2)`, where `t` (type `numpy.ndarray`) is the t -grid, and `tau1` (type `float`, default: 12.2 fs), and `tau2` (type `float`, default: 32. fs) are the two parameters with default values valid for fused silica.

As detailed in Eq. (10), by default, our propagation model FMAS-S-R implements the corresponding frequency-domain representation. However, for completeness, we also provide the implementation according to Eq. (C.1).

- Lin-Agrawal type response function [72]: The time-domain formulation of this response function, based on an improved model that takes into account the anisotropic nature of Raman scattering, reads

$$h_{\text{LA}}(t) = (1 - f_b) h_{\text{BW}}(t) + f_b \frac{2\tau_b - t}{\tau_b^2} e^{-t/\tau_b} \theta(t), \quad (\text{C.2})$$

with $h_{\text{BW}}(t)$ [see Eq. (C.1)] modeling the isotropic part of the response, $\tau_b = 96$ fs, and $f_b = 0.21$. This response model is implemented as function `h_LA(t)`, where `t` (type `numpy.ndarray`) is the t -grid.

- Hollenbeck-Cantrell type response function [73]: This elaborate response function implements the intermediate broadening model for the Raman response of silica fibers

Table C.4

Parameters defining the Raman response function h_{HC} [see Eq. (C.3)]. From left to right: number of vibrational mode (n), vibrational frequency (ω_n), mode amplitude (A_n), Lorentzian linewidth (γ_n), and Gaussian linewidth (Γ_n). Values are taken from Ref. [73].

n	ω_n ($\frac{\text{rad}}{\text{fs}}$)	A_n (-)	γ_n ($\times 10^{-3}$ fs $^{-1}$)	Γ_n ($\times 10^{-3}$ fs $^{-1}$)
1	0.010 60	1.00	1.64	4.91
2	0.018 84	11.40	3.66	10.40
3	0.043 56	36.67	5.49	16.48
4	0.068 28	67.67	5.10	15.30
5	0.087 21	74.00	4.25	12.75
6	0.093 62	4.50	0.77	2.31
7	0.115 18	6.80	1.30	3.91
8	0.130 29	4.60	4.87	14.60
9	0.149 50	4.20	1.87	5.60
10	0.157 28	4.50	2.02	6.06
11	0.175 18	2.70	4.71	14.13
12	0.203 43	3.10	2.86	8.57
13	0.228 86	3.00	5.02	15.07

Listing 2: Script demonstrating how the convenience class `PropConst` can be used to analyze a propagation constant.

```

1 import numpy as np
2 from fmas.propagation_constant import PropConst
3
4 def get_beta_fun_ESM():
5     p = np.polyid((16.89475, 0, -319.13216, 0,
6                 34.82210, 0, -0.992495, 0, 0.0010671)[::-1])
7     q = np.polyid((1.00000, 0, -702.70157, 0,
8                 78.28249, 0, -2.337086, 0, 0.0062267)[::-1])
9     c = 0.29979 # (micron/fs)
10    return lambda w: (1+p(w)/q(w))*w/c
11
12 beta_fun = get_beta_fun_ESM()
13 pc = PropConst(beta_fun)
14
15 w_Z = pc.find_root_beta2(1.3, 2.2)
16 # -- YIELDS: w_Z = 1.740823 rad/fs
17
18 w_S = 1.5 # (rad/fs)
19 w_GVM = pc.find_match_beta1(w_S, w_Z, 2.5)
20 # -- YIELDS: w_GVM = 2.019102 rad/fs
21
22 w_DW1 = 2.06 # (rad/fs)
23 dvg = pc.vg(w_DW1) - pc.vg(w_S)
24 # -- YIELDS: dvg = -0.000029 micron/fs
25
26 betas = pc.local_coeffs(w_S, n_max = 4)
27 # -- YIELDS: betas =
28 # [ 7.220, 4.8954, -0.0105, 0.0184, -0.0103]
29 # fs/mu, fs^2/mu, fs^3/mu, fs^4/mu, fs^5/mu; mu=micron

```

detailed in Ref. [73]. The time-domain representation of this model reads

$$h_{\text{HC}}(t) = \sum_{n=1}^{13} A_n e^{-\gamma_n t - \Gamma_n^2 t^2 / 4} \sin(\omega_n t) \theta(t), \quad (\text{C.3})$$

with parameter sequences $\{\omega_n\}_{n=1}^{13}$, $\{A_n\}_{n=1}^{13}$, $\{\gamma_n\}_{n=1}^{13}$, and $\{\Gamma_n\}_{n=1}^{13}$, summarized in Tab. C.4. In Eq. (C.3), each term represents a specific vibrational mode of Si_2O . The parameters in Tab. C.4 are derived from spectroscopic data obtained for a fused silica fiber [74]. This response model is implemented as function `h_HC(t)`, where `t` (type `numpy.ndarray`) is the t -grid.

The response functions defined by Eqs. (C.1,C.2) are quite generic. In contrast, the Hollenbeck-Cantrell type Raman model Eq. (C.3) is rather specific and caution is needed to ensure it is not used out of its range of applicability. An example that shows how the above Raman response functions can be used with the models implemented by `py-fmas` is provided along with the [online documentation](#).

Appendix D. Analyzing propagation constants

The design of custom propagation scenarios that either match experiments or carve out specific effects, observed during the dynamical evolution of optical pulses, typically require the analysis of a propagation constant. To assist a user in doing this, `py-fmas` provides the convenience class `PropConst`, defined in module `propagation_constant`, allowing to wrap and analyze a user defined propagation constant $\beta(\omega)$. A prerequisite for using `PropConst` is that $\beta(\omega)$ needs to be available as callable function.

A basic example illustrating some of the functionality implemented in terms of PropConst is shown in listing 2. Therein, in lines 4–10, the propagation constant $\beta(\omega) = \omega n(\omega)/c$ for an “endlessly single mode” (ESM) photonic crystal fiber [48] is defined. The enclosing function `get_beta_fun_ESM` returns a closure, implementing a rational Padé-approximant of order $[N = 8/M = 8]$ for the refractive index $n(\omega)$, as defined by Eq. (31). In line 12, $\beta(\omega)$ is initialized. It is wrapped by the convenience class in line 13. In line 15 it is shown how a zero-dispersion point, located within the bracketing interval (1.3, 2.2) rad/fs can be determined, yielding $\omega_z \approx 1.7408$ rad/fs. In line 19 it is shown how a group-velocity matched (GVM) partner frequency to $\omega_S = 1.5$ rad/fs, located in the bracketing interval ($\omega_z, 2.5$ rad/fs), can be determined, giving $\omega_{\text{GVM}} \approx 2.019$ rad/fs. The group-velocity mismatch $\Delta v_g = v_g(\omega_{\text{DW1}}) - v_g(\omega_S)$ for $\omega_{\text{DW1}} = 2.06$ rad/fs [see sect. 9.3] is calculated in line 23, yielding $\Delta v_g \approx -2.9 \cdot 10^{-5}$ $\mu\text{m}/\text{fs}$. Finally, in line 26 it is shown how the Taylor-expansion coefficients $\{\beta_n\}_{n=0}^4$ at ω_S can be obtained, yielding $\beta_0 \approx 7.220 \mu\text{m}^{-1}$, $\beta_1 \approx 4.8954 \text{ fs}/\mu\text{m}$, $\beta_2 \approx -0.0105 \text{ fs}^2/\mu\text{m}$, $\beta_3 \approx 0.0184 \text{ fs}^3/\mu\text{m}$, and $\beta_4 \approx -0.0103 \text{ fs}^4/\mu\text{m}$.

Acknowledgements

We acknowledge financial support from the Deutsche Forschungsgemeinschaft (DFG) under Germany’s Excellence Strategy within the Clusters of Excellence PhoenixD (Photonics, Optics, and Engineering – Innovation Across Disciplines) (EXC 2122, projectID 390833453).

References

- [1] A. V. Husakou, J. Hermann, Supercontinuum generation of higher-order solitons by fission in photonic crystal fibers, *Phys. Rev. Lett.* 87 (2001) 203901.
- [2] T. Brabec, F. Krausz, Nonlinear Optical Pulse Propagation in the Single-Cycle Regime, *Phys. Rev. Lett.* 78 (1997) 3282.
- [3] G. P. Agrawal, *Nonlinear Fiber Optics*, Academic Press, Boston, 2013.
- [4] Y. S. Kivshar, G. P. Agrawal, *Optical Solitons: From Fibers to Photonic Crystals*, Academic Press, San Diego, 2003.
- [5] F. Mitschke, *Fiber Optics: Physics and Technology*. Springer, Berlin, 2010.
- [6] Sh. Amiranashvili, A. Demircan, Hamiltonian structure of propagation equations for ultrashort optical pulses, *Phys. Rev. A* 82, 013812 (2010).
- [7] Sh. Amiranashvili, A. Demircan, Ultrashort Optical Pulse Propagation in terms of Analytic Signal, *Advances in Optical Technologies 2011* (2011) 989515.
- [8] Sh. Amiranashvili, Hamiltonian Framework for Short Optical Pulses, in “New Approaches to Nonlinear Waves”, Lecture Notes in Physics 908 (Ed. E. Tobisch), Springer, Heidelberg, 2016.
- [9] A. Demircan, S. Amiranashvili, C. Brée, C. Mahnke, F. Mitschke, G. Steinmeyer, Rogue wave formation by accelerated solitons at an optical event horizon, *Appl. Phys. B* 115 (2014) 343.
- [10] A. Demircan, Sh. Amiranashvili, C. Brée, U. Morgner, G. Steinmeyer, Supercontinuum generation by multiple scatterings at a group velocity horizon, *Opt. Exp.* 22 (2014) 3866.
- [11] K. E. Oughstun, H. Xiao, Failure of the Quasimonochromatic Approximation for Ultrashort Pulse Propagation in a Dispersive, Attenuative Medium, *Phys. Rev. Lett.* 78 (1997) 642.
- [12] K. E. Oughstun, *Electromagnetic and Optical Pulse Propagation 2 – Temporal Pulse Dynamics in Dispersive, Attenuative Media*, Springer, Berlin, 2009.

- [13] O. Melchert, py-fmas: Ultrashort optical pulse propagation in terms of forward models for the analytic signal, GitHub repository <https://github.com/omelchert/py-fmas>, 2020, [Online; accessed 14 April 2021].
- [14] K. J. Blow, D. Wood, Theoretical Description of Transient Stimulated Raman Scattering in Optical Fibers, *IEEE J. Quant. El.* 25 (1989) 2665.
- [15] M. Conforti, A. Marini, T. X. Tran, D. Faccio, F. Biancalana, Interaction between optical fields and their conjugates in nonlinear media, *Opt. Exp.* 21 (2013) 31239.
- [16] A. M. Zheltikov, Optical shock wave and photon-number conservation, *Phys. Rev. A* 98 (2018) 043833.
- [17] W. H. Press, William, S. A. Teukolsky, W. T. Vetterling, B. P. Flannery, *Numerical Recipes 3rd Edition: The Art of Scientific Computing*, Cambridge University Press, Cambridge, 2007.
- [18] T. R. Taha, M. J. Ablowitz, Analytical and Numerical Aspects of Certain Nonlinear Evolution Equations. II. Numerical, Nonlinear Schrödinger Equation, *J. Comp. Phys.* 55 (1984) 203.
- [19] J. A. C. Weideman, B. M. Herbst, Split-Step Methods for the Solution of the Nonlinear Schrödinger Equation, *SIAM J. Numer. Anal.* 23 (1986) 485.
- [20] P. L. DeVries, Application of the Split Operator Fourier Transform method to the solution of the nonlinear Schrödinger equation, *AIP Conf. Proc.* 160 (1987) 269.
- [21] B. García-Archilla, Some Practical Experience with the Time Integration of Dissipative Equations, *J. Comp. Phys.* 122 (1995) 25.
- [22] P. A. Milewski, E. G. Tabak, A Pseudospectral Procedure for the Solution of Nonlinear Wave Equations with Examples from Free-Surface Flows, *SIAM J. Sci. Comp.* 21 (1999) 1102.
- [23] L. N. Trefethen, *Spectral Methods in MATLAB*, SIAM, Philadelphia, 2000.
- [24] A.-K. Kassam, L. N. Trefethen, Fourth-order time-stepping for stiff PDEs, *SIAM J. Sci. Comp.* 26 (2005) 1214.
- [25] J. Hult, A Fourth-Order Runge–Kutta in the Interaction Picture Method for Simulating Supercontinuum Generation in Optical Fibers, *IEEE J. Lightwave Tech.* 25 (2007) 3770.
- [26] O. V. Sinkin, R. Holzöhner, J. Zweck, C. R. Menyuk, Optimization of the Split-Step Fourier Method in Modeling Optical-Fiber Communications Systems, *IEEE J. Lightwave Tech.* 21 (2003) 61.
- [27] A. M. Heidt, Efficient Adaptive Step Size Method for the Simulation of Supercontinuum Generation in Optical Fibers, *IEEE J. Lightwave Tech.* 27 (2009) 3984.
- [28] S. L. Marple, Computing the Discrete-Time “Analytic” Signal via FFT, *IEEE Trans. Sig. Proc.* 47 (1999) 2600.
- [29] G. Rossum, *Python Reference Manual*, Centre for Mathematics and Computer Science, Amsterdam, 1995.
- [30] E. Jones, T. Oliphant, P. Peterson, et al., SciPy: Open source scientific tools for Python, <http://www.scipy.org/>, 2001–2018, [Online; accessed 2 April 2021]
- [31] P. Virtanen, R. Gommers, T. E. Oliphant, et al., SciPy 1.0: fundamental algorithms for scientific computing in Python, *Nature Methods* 17 (2020) 261.
- [32] J. D. Hunter, Matplotlib: A 2D graphics environment, *Computing in Science & Engineering* 9 (2007) 90.
- [33] The HDF Group, Hierarchical Data Format, version 5, <http://www.hdfgroup.org/HDF5/>, 1997, [Online; accessed 2 April 2021].
- [34] A. Collette, *Python and HDF5*, O’Reilly Media, 2013.
- [35] N. J. Zabusky, M. D. Kruskal, Interaction of “Solitons” in a Collisionless Plasma and the Recurrence of Initial States, *Phys. Rev. Lett.* 15 (1965) 240.
- [36] L. A. Lugiato, R. Lefever, Spatial Dissipative Structures in Passive Optical Systems, *Phys. Rev. Lett.* 58 (1987) 2209.
- [37] O. Melchert, A. Yulin, A. Demircan, Dynamics of localized dissipative structures in a generalized Lugiato–Lefever model with negative quartic group-velocity dispersion, *Opt. Lett.* 45 (2020) 2764.
- [38] S. Balac, F. Mahé, Embedded Runge–Kutta scheme for step-size control in the interaction picture method, *Comput. Phys. Commun.* 184 (2013) 1211.
- [39] S. Balac, A. Fernandez, SPIP: A computer program implementing the Interaction Picture method for simulation of light-wave propagation in optical fibre, *Comput. Phys. Commun.* 199 (2016) 139.
- [40] O. Melchert, B. Roth, U. Morgner, A. Demircan, OptFROG — Ana-

- lytic signal spectrograms with optimized time–frequency resolution, *SoftwareX* 10 (2019) 100275.
- [41] J. W. Miles, An Envelope Soliton Problem, *SIAM J. Appl. Math.* 41 (1981) 227.
- [42] A. Demircan, U. Bandelow, Supercontinuum generation by the modulation instability, *Optics Communications* 244 (2005) 181.
- [43] A. Demircan, U. Bandelow, Analysis of the interplay between soliton fission and modulation instability in supercontinuum generation, *Appl. Phys. B*, 86 (2007) 31.
- [44] J. M. Dudley, G. Genty, S. Coen, Supercontinuum generation in photonic crystal fiber, *Rev. Mod. Phys.* 78 (2006) 1135.
- [45] P. G. Drazin, R. S. Johnson, *Solitons: An Introduction*, Cambridge University Press, Cambridge, 1989.
- [46] G. Ycas, *pyNLO: Nonlinear optics modeling for Python*, <https://github.com/pyNLO/PyNLO>, 2016, [Online; Accessed 1 April 2021].
- [47] K. E. Oughstun, Computational methods in ultrafast time-domain optics, *Computing in Science & Engineering* 5 (2003) 22.
- [48] J. M. Stone, J.C. Knight, Visibly ‘white’ light generation in uniform photonic crystal fiber using a microchip laser, *Opt. Exp.* 16 (2007) 2670.
- [49] Sh. Amiranashvili, U. Bandelow, A. Mielke, Padé approximant for refractive index and nonlocal envelope equations, *Opt. Commun.* 283 (2010) 480.
- [50] Sh. Amiranashvili, U. Bandelow, A. Mielke, Calculation of ultrashort pulse propagation based on rational approximations for medium dispersion, *Opt. Quant. Electron.* 44 (2012) 241.
- [51] A. Demircan, Sh. Amiranashvili, G. Steinmeyer, Controlling Light by Light with an Optical Event Horizon, *Phys. Rev. Lett.* 106 (2011) 16391.
- [52] R. Smith, The reflection of short gravity waves on a non-uniform current, *Math. Proc. Cambridge Philos. Soc.* 78 (1975) 517.
- [53] C. M. de Sterke, Optical push broom, *Opt. Lett.* 17 (1992) 914.
- [54] T. G. Philbin, C. Kuklewicz, S. Robertson, S. Hill, F. König, U. Leonhardt, Fiber-Optical Analog of the Event Horizon, *Science* 319 (2008) 1367.
- [55] D. Faccio, Laser pulse analogues for gravity and analogue Hawking radiation, *Cont. Phys.* 1 (2012) 1.
- [56] B. W. Plansinis, W. R. Donaldson, G. P. Agrawal, What is the Temporal Analog of Reflection and Refraction of Optical Beams?, *Phys. Rev. Lett.* 115 (2015) 183901.
- [57] A. Demircan, Sh. Amiranashvili, C. Brée, G. Steinmeyer, Compressible Octave Spanning Supercontinuum Generation by Two-Pulse Collisions, *Phys. Rev. Lett.* 110 (2013) 233901.
- [58] A. Demircan, Sh. Amiranashvili, C. Brée, U. Morgner, G. Steinmeyer, Adjustable pulse compression scheme for generation of few-cycle pulses in the midinfrared, *Opt. Lett.* 39 (2014) 2735.
- [59] R. Driben, F. Mitschke, N. Zhavoronkov, Cascaded interactions between Raman induced solitons and dispersive waves in photonic crystal fibers at the advanced stage of supercontinuum generation, *Opt. Exp.* 18 (2010) 25993.
- [60] A. Demircan, S. Amiranashvili, C. Brée, C. Mahnke, F. Mitschke, G. Steinmeyer, Rogue events in the group velocity horizon, *Sci. Rep.* 2 (2012) 850.
- [61] A. Armaroli, C. Conti, F. Biancalana, Rogue solitons in optical fibers: a dynamical process in a complex energy landscape?, *Optica* 2 (2015) 497.
- [62] O. Melchert, C. Brée, A. Tajalli, A. Pape, R. Arkhipov, S. Willms, I. Babushkin, D. Skryabin, G. Steinmeyer, U. Morgner, A. Demircan, All-optical supercontinuum switching, *Commun. Phys.* 3 (2020) 146.
- [63] J. M. Dudley, X. Gu, L. Xu, M. Kimmel, E. Zeek, P. O’Shea, R. Trebino, S. Coen, R. S. Windeler, Cross-correlation frequency resolved optical gating analysis of broadband continuum generation in photonic crystal fiber: simulations and experiments, *Opt. Exp.* 10 (2002) 1215.
- [64] D. V. Skryabin, A. V. Yulin, Theory of generation of new frequencies by mixing of solitons and dispersive waves in optical fibers, *Phys. Rev. E* 72 (2005) 016619.
- [65] D. J. Kane, R. Trebino, Characterization of Arbitrary Femtosecond Pulses Using Frequency-Resolved Optical Gating, *IEEE J. Quantum Electron.*, 29 (1993) 571.
- [66] S. Linden, J. Kuhl, H. Giessen, XFROG—Cross-correlation Frequency-resolved Optical Gating, in “Frequency-Resolved Optical Gating: The Measurement of Ultrashort Laser Pulses” (Ed. R. Trebino), Springer, Boston, 2000.
- [67] A. Efimov, A. V. Yulin, D. V. Skryabin, J. C. Knight, N. Joly, F. G. Omenetto, A. J. Taylor, P. Russell, Interaction of an Optical Soliton with a Dispersive Wave, *Phys. Rev. Lett.*, 95 (2005) 213902.
- [68] F. M. Mitschke, L. F. Mollenauer, Discovery of the soliton self-frequency shift, *Opt. Lett.* 11 (1986) 659.
- [69] J. P. Gordon, Theory of the soliton self-frequency shift, *Opt. Lett.* 11 (1986) 662.
- [70] L. Liu, G. Qin, Q. Tian, D. Zhao, W. Qin, Numerical investigation of mid-infrared supercontinuum generation up to 5 μm in single mode fluoride fiber, *Opt. Exp.* 19 (2011) 10041.
- [71] C. Agger, C. Petersen, S. Dupont, H. Steffensen, J. K. Lyngsø, C. L. Thomsen, J. Thøgersen, S. R. Keiding, O. Bang, Supercontinuum generation in ZBLAN fibers—detailed comparison between measurement and simulation, *J. Opt. Soc. Am. B* 29 (2012) 635.
- [72] Q. Lin, G. P. Agrawal, Raman response function for silica fibers, *Opt. Lett.* 31 (2006) 3086.
- [73] D. Hollenbeck, C. D. Cantrell, Multiple-vibrational-mode model for fiber-optic Raman gain spectrum and response function, *J. Opt. Soc. Am. B* 19 (2002) 2886.
- [74] R. H. Stolen, J. P. Gordon, W. J. Tomlinson, H. A. Haus, Raman response function of silica-core fibers, *J. Opt. Soc. Am. B* 6 (1989) 1159.